

Complementary Frequency Modulated Radar Waveforms and Optimised Receive Processing

Christian C. Jones^{1*}, Charles A. Mohr^{1,2}, Patrick M. McCormick², Shannon D. Blunt¹

¹Radar Systems Lab (RSL), University of Kansas, Lawrence, KS, USA

²Sensors Directorate, Air Force Research Laboratory (AFRL), WPAFB, OH, USA

*c422j868@ku.edu

Abstract: Design methodologies are developed for complementary frequency modulated (FM) waveforms and for optimized complementary mismatched filtering (MMF) of arbitrary nonrepeating waveforms. The former is a sub-class of random FM waveforms denoted as complementary FM (Comp-FM) while the latter extends a practical instantiation of Least-Squares MMF yielding the mismatched complementary-on-receive filtering (MiCRFT) scheme. Both of these approaches have an emphasis on the non-ideal physical effects of the radar transmitter and receiver, thereby permitting high-fidelity simulation analysis and subsequent experimental demonstration of their efficacy using open-air measurements.

1. Introduction

Complementary codes/sequences were originally proposed by Golay in the early 1960's [1] and have since been extensively explored (e.g. [2-16]) as a means to completely remove autocorrelation sidelobes through combining of the pulse compressed responses resulting from pairs/sets of complementary coded pulses. However, there are two factors that limit the efficacy of complementary coding in practice: Doppler sensitivity and implementation/ transmitter distortion.

Doppler sensitivity occurs because these codes are generally designed to achieve perfect sidelobe cancellation when their respective (matched or mismatched) filter responses are directly combined, which naturally corresponds to the zero-Doppler condition (subsuming compensation by a single known Doppler shift). Consequently, if a collection of scattering incurs unanticipated phase-changes due to Doppler – interpulse phase offsets, intrapulse phase ramps, or both – a deviation from the ideal condition arises that results in a commensurate regrowth of residual sidelobes (noting that some degree of cancellation may still be achieved). While sequence ordering of complementary codes was proposed as a strategy to provide more Doppler resilience [12, 15], it was noted in [16] that such an approach degrades when interpulse weighted is employed. Moreover, this method and other traditional approaches rely on the direct implementation of codes, which leads to the second limiting factor.

Limitations of complementary coding due to distortion are caused by some combination of *a*) realization of the code as a physical signal and/or *b*) distortion induced by the radar transmitter (see [16-18]). Taking these in reverse order, the rapid (theoretically instantaneous) phase changes that exist for coded waveforms exhibit extended spectral skirts that cannot be passed through a radar transmitter, which possesses some finite operational bandwidth (the passband) and associated spectral roll-off characteristics (itself a topic of ongoing research to address increasing spectral congestion [19]). Attempts to shape the spectrum through windowing or filtering (e.g. [20]) subsequently introduce amplitude

modulation (AM) that incurs further distortion (possibly severe) since high-power transmitters operate in saturation. Consequently, it is necessary in practice to employ an appropriate code-to-waveform implementation that provides some degree of spectral containment while also preserving the constant amplitude structure. In so doing, the degree of transmitter distortion can be kept to a manageable level, though it cannot be completely mitigated, particularly at high power.

Well-known methods for the implementation of binary codes as physical waveforms are derivative phase-shift keying (DPSK) [21] and the biphas-to-quadriphase (BTQ) transformation [22], which is a form of minimum shift keying (MSK). Of course, in the process of producing a physical waveform, both of these implementations necessarily modify idealized complementary codes, thereby significantly degrading the complementarity condition.

It was more recently shown in [23, 24] that the polyphase-coded frequency modulation (PCFM) code-to-waveform implementation, a form of digital FM, can be realized by modifying the communication-oriented continuous phase modulation (CPM) scheme [25] to make it suitable for radar. Consequently, PCFM provides the means with which to convert arbitrary polyphase codes into physical FM waveforms that are amenable to a radar transmitter because they possess relatively good spectral containment (no abrupt phase changes) and constant amplitude. These attributes of FM in general are part of the reason why linear FM (LFM) is still so widely used today.

It was noted in [16] that the precursor form of PCFM in [26] (and also [23, 24] by extension) likewise produces a physical waveform that deviates from the idealized structure of a code, which again is particularly problematic for complementary combining. However, these discrepancies introduced by DPSK, BTQ, and PCFM should actually not be viewed as distortions of idealized codes, but as missing components in the design of coded (i.e. parameterized) physical waveforms. From this perspective, one can then consider how to realize a complementary sidelobe cancellation condition for physical waveforms. Such an

This paper is a preprint of a paper accepted by IET Radar, Sonar & Navigation and is subject to Institution of Engineering and Technology Copyright. When the final version is published, the copy of record will be available at the IET Digital Library.

DISTRIBUTION STATEMENT A. Approved for public release: distribution unlimited.

approach is precisely what was done in [27] using PCFM, of which this paper is an expansion. Accordingly, the resulting complementary FM (Comp-FM) waveforms can be deployed in real radar systems, as experimentally demonstrated later using free-space measurements.

From a particular outlook, Comp-FM waveforms may be viewed as a generalization of complementary coding. Specifically, where the latter achieves sidelobe cancellation by exploiting the additional degrees of freedom provided by a pair of (or in general N) different waveforms, Comp-FM belongs to a growing family of “random FM” waveforms whereby every pulse possesses a unique waveform that is not repeated (see [28] for an overview). The benefit of non-repetition in this context is that, while unique subsets of waveforms can be designed for sidelobe cancellation via complementary combining, the overall coherent processing interval (CPI) is comprised of distinct subsets that provide even further sidelobe reduction by virtue of incoherent sidelobe averaging. As a result, additional resilience is obtained in practice when complementary sidelobe cancellation alone is degraded due to Doppler.

It should be noted, of course, that the use of random FM waveforms does introduce an effect denoted as range sidelobe modulation (RSM) [29, 30] that can limit the efficacy of clutter cancellation. Simply put, the pulse-to-pulse changing of range sidelobes modulates the clutter, thus introducing a nonstationarity. That said, suppression of sidelobes through Least-Squares mismatched filtering (LS-MMF) [31] appropriate for FM waveforms [23, 32-34] can be an effective compensation strategy to this problem. Therefore, because the very purpose of complementary combining is range sidelobe cancellation, the use of random FM waveforms in this context has a built-in mechanism for RSM compensation, as later demonstrated experimentally.

Another interesting attribute of random FM waveforms is that their inherent diversity enables the prospect of complementary sidelobe cancellation based on appropriate filtering of arbitrary non-repeating waveforms (such as those described in [33, 35-38]). Specifically, work by Bi and Rohling [13] on mismatched filters (MMFs) for sets of binary codes has recently been generalized [39] to permit application to random FM waveforms. In so doing, complementary combining can be achieved through the joint optimization of subsets of MMFs, thus providing an alternative to complementary waveform design. Denoted as mismatched complementary-on-receive filtering (MiCRFt), this approach can be used to place the burden of complementary design solely on the receive side, as demonstrated experimentally using free-space measurements. Moreover, it is likewise shown that the combination of Comp-FM waveforms and MiCRFt receive processing can yield even better performance (in terms of sidelobe suppression and associated RSM compensation) than either approach alone.

The remainder of the paper is organized as follows. Section 2 briefly surveys the PCFM waveform structures considered here, while Sect. 3 subsequently summarizes optimal mismatched filtering for FM waveforms. In Sect. 4 the structure, optimization approach, and some simulation results for Comp-FM waveforms are provided. Section 5 subsequently derives the MiCRFt formulation, incorporates range straddling effects, defines a mismatch loss metric, and provides additional simulation results. Finally, Sect. 6 demonstrates how these waveforms and this joint filtering

scheme perform using free-space measurements, as well as the prospective benefits of combining them.

2. FM Waveform Representation

Consider the baseband form of a constant amplitude, pulsed radar waveform having pulsewidth T , which can be generically expressed as

$$s(t) = \exp(j\phi(t)) \quad (1)$$

for $0 \leq t \leq T$ and $\phi(t)$ the instantaneous phase as a function of continuous time t . Traditional biphasic and polyphasic codes, and subsequent complementary codes that rely on these signal structures, represent the phase function as a discrete sequence $\bar{\phi}_n$ that modulates a train of rectangular “chips” (or subpulses) via

$$\phi(t) = \sum_n \bar{\phi}_n \text{rect}(t - nT_c), \quad (2)$$

where T_c is the temporal extent of each constant-phase chip. Consequently, the spectral content of these coded waveforms is a weighted sum of sinc(\bullet) functions; hence the extended spectral skirts noted in [17, 18, 23].

The DPSK and BTQ implementations [21, 22] can be used to convert binary codes ($\bar{\phi}_n \in \{0, \pi\}$) into physical waveforms with better spectral containment – note that we do not say bandlimited because a finite duration pulse still possesses theoretically infinite bandwidth. However, the use of polyphasic coding within the PCFM framework provides greater design freedom due to use of the entire 2π phase continuum. The parameterized phase function for the PCFM implementation [23] takes the form

$$\phi(t; \mathbf{x}) = \int_0^t g(\tau) * \left[\sum_{n=1}^N \alpha_n \delta(t - (n-1)T_p) \right] d\tau + \bar{\phi}_0, \quad (3)$$

where vector $\mathbf{x} = [\alpha_1 \alpha_2 \cdots \alpha_N]^T$ collects the N PCFM phase-change (instantaneous frequency) parameters $\alpha_n \in [-\pi, +\pi]$, the operation $(\bullet)^T$ is the vector transpose, and $*$ denotes convolution. The term $g(\tau)$ is a frequency shaping filter (usually rectangular with time support on $[0, T_p]$) that is convolved with the weighted impulse train in (3), where the impulses are separated by T_p and $T = NT_p$. Integration turns the resulting instantaneous frequency function into a continuous phase function that is piece-wise linear with initial phase $\bar{\phi}_0$.

The representation in (3) is the first-order PCFM implementation because it involves a single integration stage. The attributes of higher-order PCFM implementations with additional integration stages have also been examined [40], though they will not be considered here. The reader should note, however, that MatlabTM code for the various PCFM implementation orders can be found in the appendix of [40].

Evaluation of the convolution and integration operations in (3) provides the equivalent form

$$\phi(t; \mathbf{x}) = \sum_{n=1}^N \alpha_n b_n(t) + \bar{\phi}_0 \quad (4)$$

in which

$$b_n(t) = \int_0^t g(\tau - (n-1)T_p) d\tau \quad (5)$$

is the n th continuous basis function (of N). If the shaping filter is rectangular with amplitude $1/T_p$ (so it integrates to unity), then the n th basis function from (5) is the time-shifted ramp

$$b_n(t) = \begin{cases} 0, & 0 \leq t \leq (n-1)T_p \\ (t - (n-1)T_p)/T_p, & (n-1)T_p \leq t \leq nT_p \\ 1, & nT_p \leq t \leq NT_p. \end{cases} \quad (6)$$

The n th basis function can be discretised as the length- M ($>N$) vector \mathbf{b}_n , where N is also a good approximation for the waveform's time-bandwidth product BT (for B the 3-dB bandwidth) [23]. Since true Nyquist sampling cannot be achieved for a time-limited pulse, setting $M = NK$ for some "over-sampling" value K (relative to 3-dB bandwidth) allows aliasing to be kept to a minimum; with K as low as 2 or 3 generally sufficient.

Therefore, a discretised representation of the continuous phase function in (4) can be expressed as the length- M vector

$$\boldsymbol{\phi}(\mathbf{x}) = \mathbf{B}\mathbf{x} + \bar{\phi}_0, \quad (7)$$

where the $M \times N$ matrix \mathbf{B} is comprised of the N discretised basis functions. A discretised form of the corresponding PCFM waveform can likewise be expressed via (1) as

$$\mathbf{s}(\mathbf{x}) = \exp(j\boldsymbol{\phi}(\mathbf{x})), \quad (8)$$

noting that the construction above ensures abrupt phase changes are avoided. Further, if resampling is required relative to the digital-to-analog converter (DAC) rate when generating a PCFM waveform in hardware, phase interpolation (instead of standard sinc interpolation) should be used to avoid unnecessary amplitude distortion. Also, because the arbitrary initial phase $\bar{\phi}_0$ cancels when performing receiver matched filtering, we shall henceforth ignore it.

3. Optimal Mismatched Filtering - FM Waveforms

It is well known that windowing of the LFM matched filter can be used to compensate for what are otherwise rather high range sidelobes [17, 18], though this approach does not represent optimality in any sense. Conversely, it has been shown [31] that a mismatched filter that is optimal in the Least Squares sense (LS-MMF) can be determined for the abstract form of arbitrary codes (i.e. represented solely by the values in the code via (2)). That said, range straddling effects [23, 41, 42] can lead to degradation in practice due to model mismatch.

More recently, [23] demonstrated how the LS-MMF formulation could be modified for application to arbitrary FM waveforms, where the continuous nature of FM provides some natural robustness to range straddling effects. Moreover, while straddling cannot be completely avoided when performing digital receive processing, it was likewise shown [32] that simple averaging based on sub-sample delay shifts of the model can provide further robustness. Later we leverage this LS-MMF formulation for FM waveforms to establish a complementary approach based solely on receive processing. Hence a brief review is in order.

Let arbitrary FM waveform $s(t)$, with pulsewidth T and 3-dB bandwidth B , be discretised into the length- M vector \mathbf{s} according to sampling period

$$T_s = \frac{T}{K(BT)} = \frac{T}{M}, \quad (9)$$

where BT is again the time-bandwidth product and K is the same "over-sampling" factor discussed above. The original LS-MMF for codes [31] defines the $((\kappa+1)M-1) \times \kappa M$ convolution matrix

$$\mathbf{A} = \begin{bmatrix} s_1 & 0 & \cdots & 0 \\ \vdots & s_1 & & \vdots \\ s_M & \vdots & \ddots & 0 \\ 0 & s_M & & s_1 \\ \vdots & & \ddots & \vdots \\ 0 & \cdots & 0 & s_M \end{bmatrix} \quad (10)$$

and subsequently poses the relationship

$$\mathbf{A}\mathbf{h} = \mathbf{e}_m, \quad (11)$$

where κM is the length of the resulting filter (with κ typically on the order of 2 to 4), \mathbf{e}_m is the length $(\kappa+1)M-1$ elementary vector with a one in the m th element and zeros elsewhere, and \mathbf{h} is the desired MMF.

The well-known solution to (11) is

$$\mathbf{h} = (\mathbf{A}^H \mathbf{A})^{-1} \mathbf{A}^H \mathbf{e}_m, \quad (12)$$

with $(\bullet)^H$ denoting the Hermitian operation. However, as it stands, (12) does not properly account for the over-sampling that is needed to represent an FM waveform with high fidelity (i.e. minimal aliasing), and thus this form of LS-MMF produces a super-resolution condition that causes sidelobe and mismatch loss degradation [18]. That said, (12) can be readily modified to make it suitable for FM waveforms and the associated over-sampling via [23]

$$\mathbf{h} = (\tilde{\mathbf{A}}^H \tilde{\mathbf{A}} + \delta \mathbf{I})^{-1} \tilde{\mathbf{A}}^H \mathbf{e}_m. \quad (13)$$

Here $\delta \mathbf{I}$ provides diagonal loading and $\tilde{\mathbf{A}}$ is the same as \mathbf{A} except that some number of rows above and below the m th row are replaced with zeros to facilitate the "beam-spoiling" needed to prevent the range super-resolution condition. It is this form in (13) that we expand upon to design a set of mismatched filters that realize a complementary capability.

4. Complementary FM Waveforms

The compact, discretised representation of parameterized, continuous PCFM waveforms embodied by (7) and (8) permits the use of a variety of optimization approaches and the consideration of many different physically-realizable, waveform-diverse applications. For example, in [43] (with detailed derivation in [44]) gradient-descent optimization was performed and subsequently demonstrated experimentally to realize waveforms that can reach a lower bound on sidelobe performance for discretised FM waveforms. This general approach was also employed to optimize coded FM waveforms based on Legendre polynomials [45] (and also account for receiver range straddling), to efficiently incorporate spectral notches into FM waveforms [46], to realize an intermodulation-based formulation for nonlinear harmonic radar [47], and to design different sub-classes of random FM waveforms [36, 37]. Here we use gradient descent to optimize subsets of complementary FM waveforms.

4.1 Complementary FM Waveform Design

The following leverages the work in [27] to obtain subsets of complementary FM waveforms that also belong to the class of random FM waveforms. Denoting each subset as consisting of Z pulsed waveforms, the sequentially transmitted subsets comprise the total CPI of C pulses. Considering the $z = 1, 2, \dots, Z$ pulses within a particular subset (for $Z \geq 2$), parameterize the z th discretised FM waveform \mathbf{s}_z using \mathbf{x}_z based on (8). Thus our goal is to design the set of PCFM codes $\mathbf{x}_1, \mathbf{x}_2, \dots, \mathbf{x}_Z$ such that the coherent combination of autocorrelations, for the corresponding waveforms $s(t; \mathbf{x}_z)$ produced by (1) and (3), realizes a response with (ideally perfect) sidelobe cancellation.

It is convenient to use a frequency domain representation and so $M-1$ zeros are appended to the z th discretised waveform \mathbf{s}_z to form

$$\bar{\mathbf{s}}_z = [\mathbf{s}_z^T \mathbf{0}_{1 \times (M-1)}]^T, \quad (14)$$

with the corresponding $(2M-1) \times 1$ discretised frequency response therefore denoted as

$$\bar{\mathbf{s}}_{f,z} = \mathbf{D}^H \bar{\mathbf{s}}_z, \quad (15)$$

where \mathbf{D}^H is the $(2M-1) \times (2M-1)$ discrete Fourier transform (DFT) matrix and \mathbf{D} is the inverse DFT matrix. Therefore, complementary combining for the set of Z waveforms yields the length- $(2M-1)$ discretised aggregate autocorrelation that can be written as

$$\mathbf{r} = [r_{-M+1} \ \dots \ r_0 \ \dots \ r_{M-1}]^T = \sum_{z=1}^Z \mathbf{D}(\bar{\mathbf{s}}_{f,z} \odot \bar{\mathbf{s}}_{f,z}^*), \quad (16)$$

in which $(\bullet)^*$ denotes complex conjugation and \odot is the Hadamard product.

Minimisation of the complementary aggregated sidelobes in (16) is a non-convex problem and global optimality cannot be guaranteed. However, in keeping with the spirit of random FM waveforms [28], it is not the single best solution we seek, but rather a diverse set of sufficiently good solutions that further benefit from incoherent sidelobe combining when slow-time (Doppler) processing is subsequently performed. Therefore, instead of an optimal, yet brittle, result that is sensitive to degradation when inevitable mismatch arises, we obtain a sub-optimal result that is more robust to these mismatch effects by virtue of simple coherent averaging.

Consequently, we shall use the generalised integrated sidelobe level (GISL) metric from [43, 44] defined as

$$J = \frac{\|\mathbf{w}_{\text{SL}} \odot \mathbf{r}\|_p}{\|\mathbf{w}_{\text{ML}} \odot \mathbf{r}\|_p}, \quad (17)$$

in which $\|\bullet\|_p$ denotes the p -norm for $p \geq 2$, and the length- $(2M-1)$ vectors \mathbf{w}_{ML} and \mathbf{w}_{SL} are each composed of ones and zeros that extract the respective mainlobe and sidelobe regions of the autocorrelation \mathbf{r} . For the PCFM construction above, the null-to-null width of the mainlobe comprises the $(2K-1)$ samples in the center of \mathbf{r} , which therefore correspond to the only values in \mathbf{w}_{ML} that are set to one (with the rest zero), and subsequently $\mathbf{w}_{\text{SL}} = \mathbf{1} - \mathbf{w}_{\text{ML}}$. It was demonstrated in [45] that setting the width of the mainlobe in this way also establishes the 3-dB bandwidth.

For each complementary subset of Z waveforms there are therefore NZ parameters to optimize with respect to (17). For the z th waveform the $N \times 1$ gradient vector is

$$\nabla_{\mathbf{x}_z} = \left[\frac{\partial}{\partial \alpha_{1,z}} \quad \frac{\partial}{\partial \alpha_{2,z}} \quad \dots \quad \frac{\partial}{\partial \alpha_{N,z}} \right]^T, \quad (18)$$

which is comprised of partial derivatives with respect to each of the N phase-change parameters. Leveraging the gradient formulation in [43] (with detailed derivation in [44]), of which (16) is a direct extension by virtue of the summation of Z autocorrelations, realizes the gradient [27]

$$\nabla_{\mathbf{x}_z} J = 2\bar{\mathbf{B}}^T \Im \left\{ \bar{\mathbf{s}}_z^* \odot \left(\mathbf{D} \left[\bar{\mathbf{s}}_{f,z} \odot \left\{ \mathbf{D}^H (\mathbf{w}_T \odot \mathbf{d} \odot \mathbf{r}) \right\} \right] \right) \right\} \quad (19)$$

for the z th of Z waveforms. Here the basis function matrix \mathbf{B} from (7) has also been appended with $M-1$ rows of zeros as

$$\bar{\mathbf{B}} = \left[\mathbf{B}^T \ \mathbf{0}_{N \times (M-1)} \right]^T \quad (20)$$

to be consistent with (14) and the operator $\Im\{\bullet\}$ extracts the imaginary part of the argument. The length- $(2M-1)$ vectors that are Hadamard multiplied with \mathbf{r} in (19) are

$$\mathbf{d} = \left[|r_{-M+1}|^{p-2} \ \dots \ |r_0|^{p-2} \ \dots \ |r_{M-1}|^{p-2} \right]^T \quad (21)$$

and

$$\mathbf{w}_T = \frac{\|\mathbf{w}_{\text{SL}} \odot \mathbf{r}\|_p}{\|\mathbf{w}_{\text{ML}} \odot \mathbf{r}\|_p} \left[\left(\frac{1}{\|\mathbf{w}_{\text{SL}} \odot \mathbf{r}\|_p^p} \right) \mathbf{w}_{\text{SL}} - \left(\frac{1}{\|\mathbf{w}_{\text{ML}} \odot \mathbf{r}\|_p^p} \right) \mathbf{w}_{\text{ML}} \right], \quad (22)$$

which arise from the gradient derivation. The gradient expression in (14) permits computation using fast Fourier transforms (FFTs) and matrix/vector multiplication [44, 48].

The gradient of (19) can thus be used to perform a descent-based optimization update for each of the Z parameter vectors \mathbf{x}_z . At the i th iteration for the z th waveform this update is

$$\mathbf{x}_{z,i+1} = \mathbf{x}_{z,i} + \mu_{z,i} \mathbf{p}_{z,i}, \quad (23)$$

where $\mu_{z,i}$ is the current step-size and the current descent direction is

$$\mathbf{p}_{z,i} = \begin{cases} -\nabla_{\mathbf{x}_{z,i}} J & \text{when } i = 0 \\ -\nabla_{\mathbf{x}_{z,i}} J + \beta \mathbf{p}_{z,i-1} & \text{otherwise} \end{cases} \quad (24)$$

for $0 \leq \beta < 1$, where we have chosen to use the heavy-ball descent method [49] and the step-size is determined via a back-tracking method [50]. Further discussion of these selections can be found in [44].

Note that each iteration of (23) is performed concurrently for the set of Z waveforms, based on the aggregate discretised autocorrelation \mathbf{r} from (16) and the subsequent gradient from (19), which are dependent on the set of updated waveforms obtained in the previous iteration. Further, to provide the needed diversity within each subset and across the distinct subsets, each PCFM waveform is independently initialized with a random instantiation of \mathbf{x} , with the individual values independently drawn from a uniform distribution on $[-\pi, +\pi]$.

Finally, while this complementary FM waveform design approach relies on the gradient-descent formulation developed in [43, 44], there are two important (and related) distinctions to make regarding implementation. The most obvious of these is that here we are making use of the degrees of freedom from Z different waveforms in a collective manner, as opposed to the optimization of a single waveform in [43, 44]. The relevant consequence of that difference is that the

single-waveform optimization in [43, 44] subsequently requires use of “over-coding” (see [51]), which provides an expansion of available degrees of freedom, to achieve sidelobe performance commensurate with that observed here. However, expansion of spectral content can arise as an undesired by-product of over-coding, thus necessitating further spectral containment measures. In contrast, the access to greater degrees of freedom afforded by complementary design avoids the spectral expansion issue altogether.

4.2 Simulation Analysis

To illustrate the efficacy of the Comp-FM framework to produce FM (and thus physically realizable) waveforms possessing complementary attributes, two distinct sets of $C = 1000$ random FM waveforms were generated. For both sets, each waveform has a 3-dB bandwidth of $B = 33.3$ MHz and a pulsewidth of $T = 4.5$ μs , thereby realizing a time-bandwidth product of $BT = 150$. Each waveform is also discretised using an over-sampling factor of $K = 6$ (relative to B), thus yielding a vector of length $N = K(BT) = 900$.

The first set serves as a non-complementary baseline and consists of $C = 1000$ pseudo-random optimized (PRO) FM waveforms that are each designed to approximate a Gaussian power spectrum, but are otherwise unique due to independent initializations (see [33]). The other set consists of $C/Z = 250$ unique subsets of $Z = 4$ Comp-FM waveforms.

Figure 1 illustrates the relative range sidelobe performance of individual PRO-FM and Comp-FM waveforms after matched filtering, as well as the aggregated autocorrelations obtained when coherently combining respective subsets of four for zero Doppler (i.e. averaging the autocorrelations from four different waveforms). Corresponding peak sidelobe level (PSL) values for each are summarized in Table I. For the individual waveform comparison, PRO-FM achieves a PSL of -27.4 dB, which is 7 dB lower than the -20.4 dB for Comp-FM. However, while the combination of four unique PRO-FM autocorrelations realizes about $10 \log_{10}(4) = 6$ dB of additional sidelobe suppression due to incoherent averaging (5.7 dB here, to be exact), the combining of $Z = 4$ Comp-FM autocorrelations achieves 34.7 dB of additional sidelobe cancellation (to -55.1 dB) due to complementarity.

Figure 2 then demonstrates the benefit of coherently combining autocorrelations over the entire set of $L = 1000$ unique waveforms. Now PRO-FM realizes a PSL of -57.3 dB due to the roughly $10 \log_{10}(1000) = 30$ dB of incoherent sidelobe averaging relative to the single waveform result in Fig. 1. Similar combining for Comp-FM over the 250 unique subsets corresponds to $10 \log_{10}(250) = 24$ dB, with the simulated result in Fig. 2 revealing a relatively close approximation of 21 dB of incoherent sidelobe averaging on top of the complementary sidelobe cancellation, thereby achieving a final PSL of -76.1 dB. Thus, despite Comp-FM having a 7-dB PSL disadvantage relative to PRO-FM on the single-waveform basis, it ends up with an 18.8-dB PSL advantage after combining over the entire set of 1000 unique waveforms.

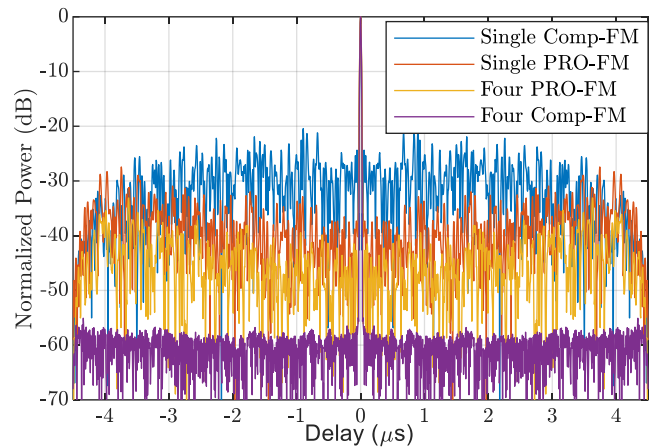


Fig. 1. Simulated autocorrelations for a single Comp-FM waveform and a single PRO-FM waveform, along with the coherent sum of autocorrelations for 4 unique PRO-FM waveforms and for a subset of $Z = 4$ Comp-FM waveforms.

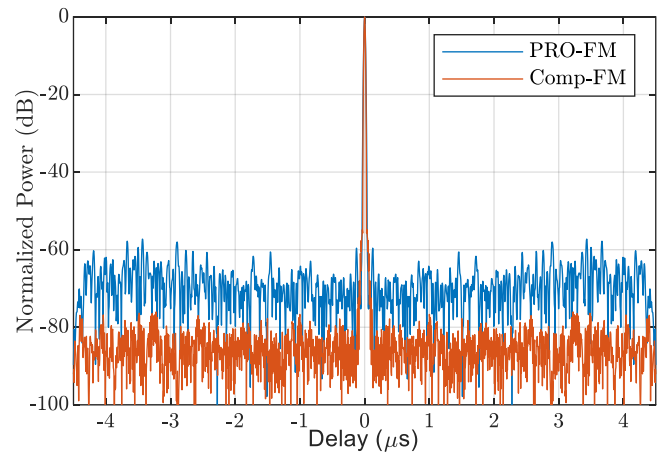


Fig. 2. Simulated coherent sum of autocorrelations for 1000 unique PRO-FM waveforms and for 250 unique subsets of $Z = 4$ Comp-FM waveforms.

Table I. PSL comparison after autocorrelation combining

Waveform	Combining	PSL
PRO-FM	none (single waveform)	-27.4 dB
Comp-FM	none (single waveform)	-20.4 dB
PRO-FM	average of 4	-33.1 dB
Comp-FM	$Z = 4$ subset	-55.1 dB
PRO-FM	CPI of $C = 1000$	-57.3 dB
Comp-FM	$C/Z = 250$ unique $Z = 4$ subsets	-76.1 dB

In Fig. 3 the power spectral density (PSD) averaged over each set of $C = 1000$ waveforms is shown. For the PRO-FM case, where each waveform is designed to approximate a Gaussian power spectrum, the resulting average is clearly rather close to a Gaussian. In contrast, no overt spectral shaping was employed for the Comp-FM design process, though the “over-sampling” (by K) of the N -dimensional parameter space for each waveform does provide a natural degree of spectral containment. It is therefore interesting to observe here that the top 25 dB of the spectral content for Comp-FM tends toward a Gaussian shape as well, though this result is not all that surprising in hindsight given that the inverse Fourier transform of a Gaussian PSD is a Gaussian

autocorrelation, which theoretically possesses no range sidelobes (and the sidelobes in Fig. 2 are quite low).

Finally, to draw a comparison between Comp-FM and traditional complementary coding schemes, the resulting value of PSL was determined as a function of pulse-to-pulse Doppler phase shift. For this comparison we considered a polyphase complementary set comprised of two length-10 codes [16], along with a subset of $Z = 2$ Comp-FM waveforms and a subset of $Z = 4$ Comp-FM waveforms.

Figure 4 depicts the results of this Doppler tolerance analysis, where the polyphase complementary set clearly experiences the most degradation as Doppler increases. The $Z = 2$ Comp-FM case provides far less sidelobe cancellation at zero Doppler, but then is relatively robust to increasing Doppler. The $Z = 4$ Comp-FM case is then a little more sensitive to Doppler (relative to $Z = 2$), but since it achieves so much better cancellation at zero Doppler it remains the best over the Doppler interval considered. While these results are clearly only anecdotal, they do indicate a general tendency towards better Doppler robustness for Comp-FM waveforms.

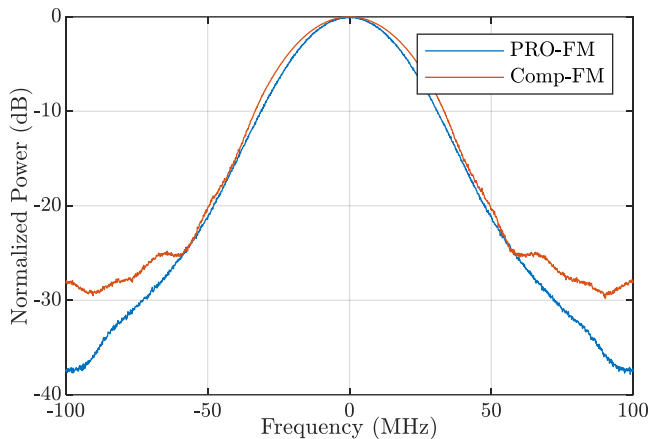


Fig. 3. Power spectral density averaged over the PRO-FM and Comp-FM sets of 1000 unique waveforms.

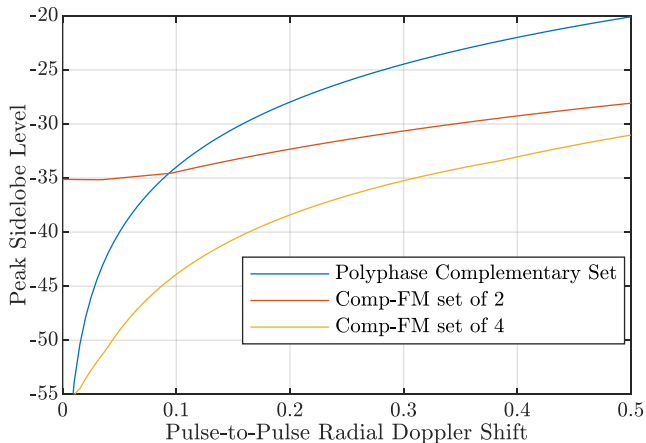


Fig. 4. PSL vs. Doppler for a polyphase complementary set of two length-10 codes compared to $Z = 2$ and $Z = 4$ Comp-FM waveform subsets.

5. Complementary MMF for FM Waveforms

The complementary sidelobe cancellation concept has historically focused almost exclusively on the design of codes that achieve this condition when combined after pulse compression. A notable exception is the work of Bi and

Rohling [13] which considers how the original LS-MMF of [31] could be incorporated to provide greater freedom in the design of complementary binary codes. Here we take this interesting idea a step further by relaxing the waveform design portion altogether (from the complementary perspective) and focusing instead on what can be achieved solely via receive filtering. In so doing, we also consider how robustness to range straddling can likewise be incorporated.

5.1 Complementary Design of Joint MMFs

Consider the design of LS-MMFs for Q diverse FM waveforms such that, when the respective filter responses are combined, a complementary condition is achieved. This approach is denoted as mismatched complementary-on-receive filtering, or MiCRFt (pronounced like “Mycroft” Holmes, fictional elder brother of Sherlock Holmes).

Returning to the LS formulation of (11), albeit with inclusion of the beam-spoiling modification within each convolution matrix as employed in (13), we can express this multiple MMF design problem as

$$\sum_{q=1}^Q \tilde{\mathbf{A}}_q \mathbf{h}_q = \mathbf{Q} \mathbf{e}_m, \quad (25)$$

where scaling of the elementary vector \mathbf{e}_m by Q accounts for coherent integration gain over the subset. This form can be rearranged into a single matrix/vector multiplication via

$$\mathbf{F} \bar{\mathbf{h}} = \mathbf{Q} \mathbf{e}_m, \quad (26)$$

in which

$$\bar{\mathbf{h}} = [\mathbf{h}_1^T \mathbf{h}_2^T \cdots \mathbf{h}_Q^T]^T \quad (27)$$

$$\mathbf{F} = [\tilde{\mathbf{A}}_1 \tilde{\mathbf{A}}_2 \cdots \tilde{\mathbf{A}}_Q] \quad (28)$$

are a length- κMQ concatenation of MMFs and a concatenated matrix with dimensionality $(\kappa + 1)M - 1 \times \kappa MQ$, respectively.

Since (26) has the same general form as (11), the collection of Q MiCRFt MMFs for this subset of diverse FM waveforms can be obtained by direct application of (13) as

$$\bar{\mathbf{h}} = \mathbf{Q} (\mathbf{F}^H \mathbf{F} + \delta \bar{\mathbf{I}})^{-1} \mathbf{F}^H \mathbf{e}_m, \quad (29)$$

where the expanded identity matrix $\bar{\mathbf{I}}$ is $\kappa MQ \times \kappa MQ$. Note that this solution necessarily requires Q diverse waveforms. In the degenerate case where the Q waveforms are identical, (25) reverts back to (11) and thus only one MMF is obtained. Moreover, if the Q waveforms are different, yet still somewhat similar (e.g. [52]), some degree of ill-conditioning in (29) may arise. Hence, the diversity from fully unique waveforms are key.

5.2 Incorporating Range Straddling into MiCRFt

Range straddling (or cusping) [41, 42] occurs when digital receive processing is performed and it arises from the fact that Nyquist sampling cannot be achieved for a time-limited pulse, which has a theoretically infinite bandwidth. Consequently, the receive-captured version of a waveform produced by a hypothetical point scatterer will generally not be sampled in precisely the same way as the discretised version used to perform matched/mismatched filtering. Thus the theoretical peak value of the pulse compression mainlobe is not obtained, which subsequently incurs mismatch loss. Further, for optimized MMFs, model mismatch effects arise

that cause increased sidelobes relative to the optimal (delay-aligned) condition.

While using a higher “over-sampling” factor in the receiver analog-to-digital converter (ADC) is an obvious solution, there tend to be practical limits on ADC rates given a prescribed quantisation bit depth. Moreover, one would also have to contend with increased noise and interference in the receiver front-end. Consequently, we shall consider how to improve robustness to straddling mismatch within the joint MMF formulation itself (in contrast to the *a posteriori* MMF averaging approach previously examined in [32] for an individual MMF).

Segment the sampling period T_s from (9) into delay offsets $\ell T_s/L$ for $\ell = 0, 1, \dots, L-1$ that are equally spaced. After introducing each of these delay offsets, subsequent discretisation of continuous waveform $s(t - \ell T_s/L)$ using the same sampling period produces a set of L length- M vectors for the q th waveform that we shall denote as $\mathbf{s}_{q,\ell}$. From these vectors corresponding beam-spoiled convolution matrices $\tilde{\mathbf{A}}_{q,\ell}$ can be formed. Thus (25) can be written for the ℓ th delay offset as

$$\sum_{q=1}^Q \tilde{\mathbf{A}}_{q,\ell} \mathbf{h}_q = Q \mathbf{e}_m \quad (30)$$

and the collection of L delay offsets can be assembled into

$$\mathbf{G} \bar{\mathbf{h}} = Q \bar{\mathbf{e}}_m. \quad (31)$$

Here

$$\bar{\mathbf{e}}_m = [\mathbf{e}_m^T \mathbf{e}_m^T \cdots \mathbf{e}_m^T]^T \quad (32)$$

is a concatenation of L elementary vectors and the matrix

$$\mathbf{G} = \begin{bmatrix} \tilde{\mathbf{A}}_{1,0} & \tilde{\mathbf{A}}_{2,0} & \cdots & \tilde{\mathbf{A}}_{Q,0} \\ \tilde{\mathbf{A}}_{1,1} & \tilde{\mathbf{A}}_{2,1} & \cdots & \tilde{\mathbf{A}}_{Q,1} \\ \vdots & \vdots & \ddots & \vdots \\ \tilde{\mathbf{A}}_{1,L-1} & \tilde{\mathbf{A}}_{2,L-1} & \cdots & \tilde{\mathbf{A}}_{Q,L-1} \end{bmatrix} \quad (33)$$

has dimensionality $((\kappa+1)M-1)L \times \kappa MQ$.

Since (31) again has the same form as (11), the solution likewise follows directly from (13) as

$$\bar{\mathbf{h}} = Q(\mathbf{G}^H \mathbf{G} + \delta \mathbf{I})^{-1} \mathbf{G}^H \bar{\mathbf{e}}_m. \quad (34)$$

Like (29), note that (34) still only produces Q MMFs, though each one is now more robust to straddling effects. Also like (29), the formulation in (34) involves a rather large $\kappa MQ \times \kappa MQ$ matrix inverse that may be computationally formidable even when using waveforms with a modest BT . Thus ongoing work is also exploring ways in which to obtain these filters, or sub-optimal versions thereof, in a more efficient manner.

5.3 MMF Normalization and Mismatch Loss

Because the MiCRFt filters are MMFs, it is necessary to consider their mismatch loss as well as the resulting sidelobe response. Determining the mismatch loss first requires normalization of the set of MMFs so that, relative to the matched filter, the same noise gain is obtained. For discretised waveform \mathbf{s} , the normalized matched filter (NMF) can be readily obtained via

$$\mathbf{h}_{\text{NMF}} = \frac{\mathbf{s}^{B*}}{\mathbf{s}^H \mathbf{s}}, \quad (35)$$

for $(\bullet)^B$ the backwards operator that reverses the signal in time. By extension, a single noise-gain normalized MMF (NMMF), relative to \mathbf{h} in (12) or (13), can be expressed as

$$\mathbf{h}_{\text{NMMF}} = \frac{\mathbf{h}}{\sqrt{(\mathbf{h}^H \mathbf{h})(\mathbf{s}^H \mathbf{s})}}. \quad (36)$$

Thus

$$\text{mismatch loss} = \frac{\max(|\mathbf{s} * \mathbf{h}_{\text{NMMF}}|)}{\max(|\mathbf{s} * \mathbf{h}_{\text{NMF}}|)} \quad (37)$$

for $*$ denoting convolution, where the denominator is actually unity via (35) and can therefore be ignored.

This definition can likewise be extended for the multi-MMF formulation of MiCRFt under the assumption that the Q waveforms in the subset have the same BT . Therefore, using the set of Q filters determined by either (29) or (34), the corresponding set of Q NMMFs can be obtained via

$$\bar{\mathbf{h}}_{\text{NMMF}} = \frac{\bar{\mathbf{h}}}{\frac{1}{Q} \sqrt{\left(\sum_{q=1}^Q \mathbf{h}_q^H \mathbf{h}_q \right) \left(\sum_{q=1}^Q \mathbf{s}_q^H \mathbf{s}_q \right)}} = \frac{Q \bar{\mathbf{h}}}{\sqrt{(\bar{\mathbf{h}}^H \bar{\mathbf{h}})(\bar{\mathbf{s}}^H \bar{\mathbf{s}})}}, \quad (38)$$

in which, like (27),

$$\bar{\mathbf{s}} = [\mathbf{s}_1^T \mathbf{s}_2^T \cdots \mathbf{s}_Q^T]^T \quad (39)$$

is the concatenation of the Q discretised waveforms. Thus

$$\begin{aligned} \text{mismatch loss} &= \frac{\sum_{q=1}^Q \max(|\mathbf{s}_q * \mathbf{h}_{\text{NMMF},q}|)}{\sum_{q=1}^Q \max(|\mathbf{s}_q * \mathbf{h}_{\text{NMF},q}|)} \\ &= \frac{1}{Q} \sum_{q=1}^Q \max(|\mathbf{s}_q * \mathbf{h}_{\text{NMMF},q}|) \end{aligned} \quad (40)$$

since each term in the denominator is still unity. Further, because (40) corresponds to the particular Q waveforms in a given subset of the larger CPI, the same procedure must be performed over the entire collection of C/Q subsets and the results subsequently averaged to determine the overall mismatch loss for the C waveforms in a CPI.

5.4 Simulation Analysis

Consider a subset of $Q = 4$ arbitrary PRO-FM waveforms with $BT = 150$ and $K = 6$ (so $N = 900$). To draw consistent comparisons between individually optimized MMFs from (13) and a given version of MiCRFt, each is parameterized with $(K-1) = 5$ rows of zeroes above and below the m th row for beamspoiling of the convolution matrices, a value of $\kappa = 2$ (so each MMF is length $2M$), and a diagonal loading factor of $\delta = 10$. The total response from a hypothetical noise-free point scatterer is evaluated using the different filtering strategies, which involves coherently combining the individual responses from Q filter/waveform pairs. Here we consider the PSL, the integrated sidelobe level (ISL), and the mismatch loss (MML) via (37) or (40) as appropriate.

Figure 5 and Table II first consider the idealized case in which the receive sampling is perfectly aligned (i.e. no range

straddling). The combination of matched filter (MF) responses for four unique waveforms realizes no mismatch loss, as expected, and a PSL of -33.1 dB. The combination of four individually optimized MMFs via (13) realizes 2.0 dB of mismatch loss, but achieves a PSL of -43.8 dB, a nearly 11-dB improvement. Most significantly, however, MiCRFt from (29) realizes a PSL of -78.2 dB (a 45-dB improvement over the MF!) with only 0.2 dB of mismatch loss.

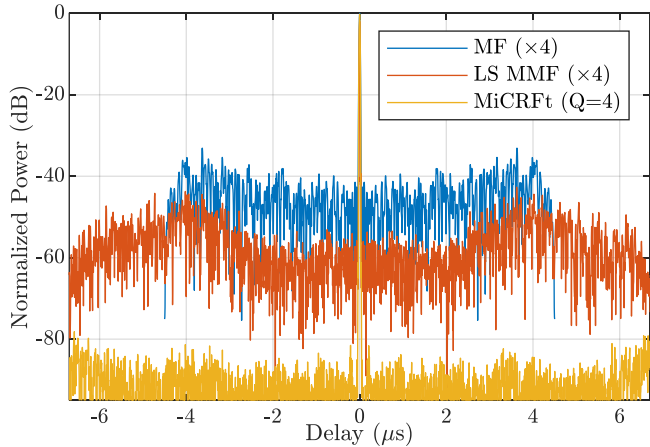


Fig. 5. Comparison of combined pulse compression responses for 4 PRO-FM waveforms with no straddling (noise-free hypothetical point scatterer)

Table II. Quantitative filter comparison of Fig. 5 ($Q = 4$)

Filter	PSL	ISL	MML
MF $\times 4$	-33.1 dB	-46.4 dB	0 dB
LS via (13) $\times 4$	-43.8 dB	-58.9 dB	2.0 dB
MiCRFt via (29)	-78.2 dB	-92.8 dB	0.2 dB

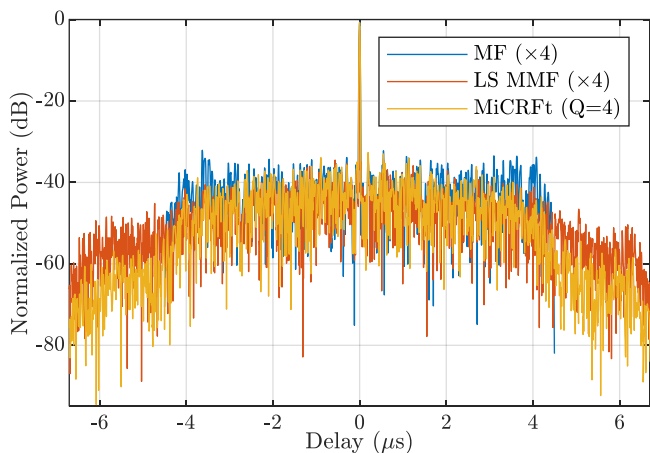


Fig. 6. Comparison of combined pulse compression responses for 4 PRO-FM waveforms with maximum straddling of $T_s/2$ (noise-free hypothetical point scatterer)

Table III. Quantitative filter comparison of Fig. 6 ($Q = 4$)

Filter	PSL	ISL	MML
MF $\times 4$	-32.1 dB	-43.4 dB	0.6 dB
LS via (13) $\times 4$	-34.5 dB	-51.1 dB	2.6 dB
MiCRFt via (29)	-33.9 dB	-53.7 dB	0.8 dB

In contrast to the ideal condition of no straddling, Fig. 6 and Table III reveal the degree of degradation that occurs when maximum straddling of $T_s/2$ is present. While the

matched filters exhibit only a 1-dB increase in PSL, they also experience a 0.6-dB mismatch loss that is completely attributable to range straddling. On the other hand, the individually optimized MMFs from (13) incur more than 9 dB in PSL degradation, along with an additional 0.6 dB of mismatch loss. Finally, in large part because the ideal results in Fig. 5 and Table II were so good to begin with, MiCRFt suffers a quite significant 44-dB degradation in PSL, as well as the same 0.6 dB in further mismatch loss. Of course, MiCRFt still has almost 2 dB lower sidelobes than the matched filters and nearly 2 dB less mismatch loss than the individual MMFs.

Finally, Fig. 7 and Table IV illustrate the benefit of using the version of MiCRFt from (34) that compensates for range straddling. Here $L = 2$ is used, so that the worst-case straddling for MiCRFt now becomes $T_s/4$ (halfway between delay offsets considered in the filter formulation). To ensure a fair comparison, similar compensation was performed for the individual MMFs by applying (34) with $L = 2$ and $Q = 1$.

The MF results are now more similar to the no-straddling case, albeit with a small 0.2-dB mismatch loss. The individual compensated MMFs do recover about 3 dB of straddling-induced sidelobe degradation, along with the original (rather high) mismatch loss of 2.0 dB. Finally, compensated MiCRFt reduces the straddling-induced mismatch loss by 0.2 dB, though the more significant improvement is in regaining more than 22 dB of sidelobe suppression. While not quite as good as in the no-straddling case, the -56.2 -dB PSL attained by compensated MiCRFt is still rather substantial given that it is under the (now) worst-case straddling condition.

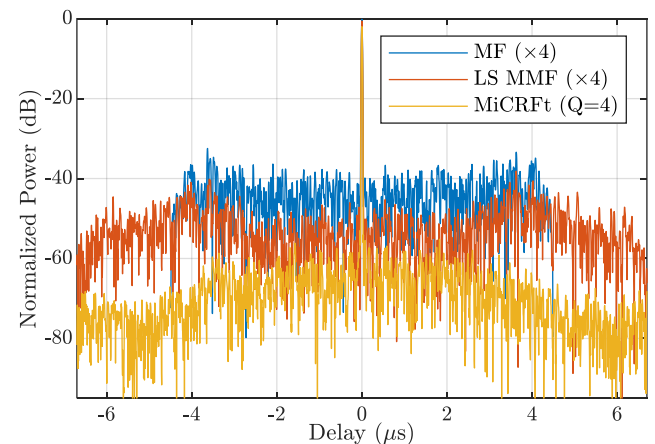


Fig. 7. Comparison of combined pulse compression responses for 4 PRO-FM waveforms using compensated MiCRFt from (34) with $L = 2$, for new maximum straddling of $T_s/4$ (noise-free hypothetical point scatterer)

Table IV. Quantitative filter comparison of Fig. 7 ($Q = 4$)

Filter	PSL	ISL	MML
MF $\times 4$	-32.5 dB	-45.3 dB	0.2 dB
LS via (34) $\times 4$	-37.8 dB	-54.4 dB	2.0 dB
MiCRFt via (34)	-56.2 dB	-71.0 dB	0.6 dB

For subsequent experimental results in the next section, (34) using $L = 2$ is employed for MiCRFt and for the individual optimized MMFs (by setting $Q = 1$). Some modest further robustness to straddling can be achieved by further increasing the value of L , though diminishing improvement is reached

rather quickly. It is therefore questionable whether the slight enhancement is worth the additional computational cost.

6. Experimental Results

The same sets of 1000 PRO-FM and Comp-FM waveforms evaluated via simulation in Sections 4.2 and 5.4 were implemented on test equipment to assess the efficacy of complementary FM waveforms and complementary-on-receive MMF using experimental measurements. We first performed a loopback assessment to determine the impact of hardware separate from the effects of scattering phenomenology. Then open-air data was collected that included multiple movers in the scene, thereby providing some sense of the resilience to Doppler effects in practice.

6.1 Closed-Loop Experimental Assessment

As before, 1000 PRO-FM and Comp-FM waveforms were designed to have pulsewidth $T = 4.5 \mu\text{s}$ and 3-dB bandwidth $B = 33.3 \text{ MHz}$. Each waveform set was generated using a Tektronix AWG70002A arbitrary waveform generator (10-bit depth) at a pulse repetition frequency (PRF) of 5 kHz and at a centre frequency of 3.55 GHz. The AWG was connected to a class A amplifier, which for this loopback configuration was connected to an attenuator and then directly into the receive chain. The latter consisted of a low-noise amplifier followed by a Rhode & Schwarz FSW26 spectrum analyser that digitized the subsequent baseband signal at a rate of 200 Megasamples/second.

The 250 Comp-FM waveform subsets of size $Z = 4$ are first pre-summed after pulse compression to obtain the complementary sidelobe cancellation. Doppler processing is then performed, where the corresponding effective PRF of 1.25 kHz does reduce the Doppler space by a factor of 4. To provide consistent results for comparison, the same pre-summing procedure is also applied to the pulse compressed PRO-FM waveforms (using MF or MMF) prior to Doppler processing. Pre-summing is likewise performed when MiCRFt is applied, where $Q = 4$ is used for simplicity (and so Comp-FM and MiCRFt can be easily combined). The individual MMFs and MiCRFt filters are generated via (34) using the loopback-captured version of each waveform, and otherwise the same parameterization discussed in Sect. 5.4.

Note that individual MMFs are not formed for the Comp-FM waveforms because doing so removes the complementary attribute for which they are designed. Thus the five filter/waveform combinations being considered are matched filtering of PRO-FM (MF / PRO-FM), matched filtering of Comp-FM (MF / Comp-FM), individually optimized MMFs applied to PRO-FM (LS-MMF / PRO-FM), MiCRFt applied to PRO-FM (MiCRFt / PRO-FM), and then the final combination (MiCRFt / Comp-FM) that doubly exploits complementarity.

Figure 8 and Table V illustrate these five combinations for a $Z = Q = 4$ subset using the loopback-captured measurements, which represent a noise-free point-scatterer response in the presence of whatever distortion the hardware imposes. The results are generally consistent with the corresponding simulation results in Figs. 1 and 5, where the most severe sidelobe degradations caused by range straddling have been largely mollified by the quasi-bandlimiting of the hardware and subsequent use of the loopback-captured versions of the waveforms to construct the receive filters,

which generally always tends to be a good idea. Consequently, the values in Table V are quite similar to the no-straddling case in Table II, despite no effort being made to perfectly synchronize the receive sampling. It should be noted, however, that spectral splatter (i.e. spreading) induced by nonlinear effects in high-power transmitters [53] can make straddling compensation even more necessary.

Most significantly, the combination of Comp-FM and MiCRFt yields extremely low sidelobes (PSL of -85.6 dB) as well as almost negligible mismatch loss. This latter observation makes sense when one considers that, since Comp-FM waveforms are designed to be combined in complementary fashion, the jointly optimized MiCRFt filters that are designed for the same purpose would not tend to cause much mismatch deviation when suppressing the sidelobes further.

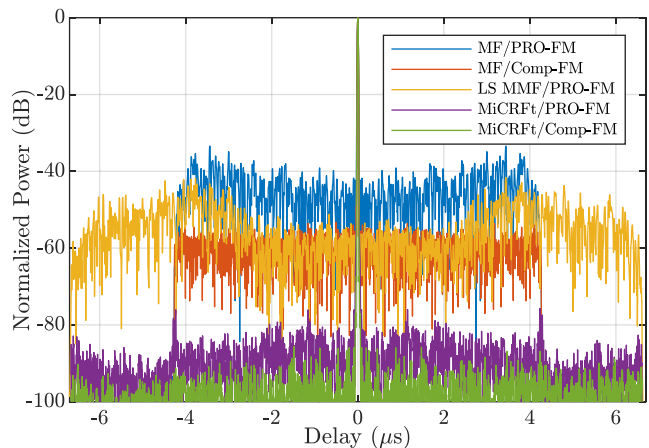


Fig. 8. Loopback measured filter responses for a single $Z = Q = 4$ subset of PRO-FM or Comp-FM

Table V. Quantitative filter comparison of Fig. 8 ($Q = 4$)

Filter / Waveform	PSL	ISL	MML
MF / PRO-FM	-33.4 dB	-50.4 dB	0 dB
MF / Comp-FM	-53.3 dB	-64.5 dB	0 dB
LS-MMF / PRO-FM	-41.9 dB	-57.1 dB	0.5 dB
MiCRFt / PRO-FM	-76.0 dB	-92.1 dB	0.4 dB
MiCRFt / Comp-FM	-85.6 dB	-101.1 dB	0.04 dB

6.2 Open-Air Experimental Assessment

Finally, free-space measurements using each set of 1000 waveforms were made from the roof of Nichols Hall on the University of Kansas campus. The AWG and amplifier were connected to a transmitting dish antenna pointed towards the intersection of 23rd and Iowa Streets in Lawrence, KS (about 1 km away), while a second nearby dish antenna was used to receive the subsequent reflections. A visualisation of this arrangement courtesy of Google Earth is depicted in Fig. 9.

The zero-Doppler slice in Fig. 10 illustrates the response of each of these five filter/waveform combinations, where the only observable difference (thus far) lies in the region between 200-300 meters and generally agrees with the PRO-FM sidelobe response in Fig. 2 after coherently combining 1000 unique waveforms. These residual sidelobes are relative to the direct path leakage between the transmit and receive antennas, which as the strongest response has been normalized to 0 dB in the figure.

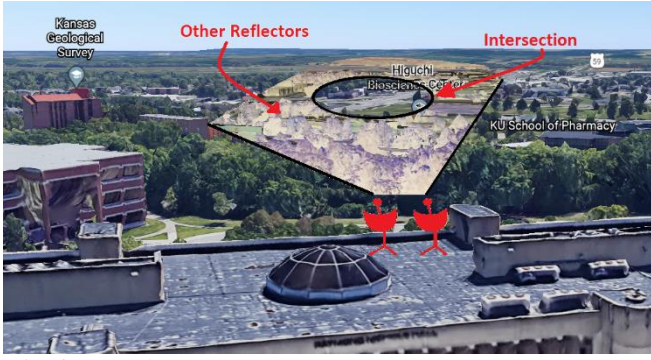


Fig. 9. Visualization of test setup for open-air measurements

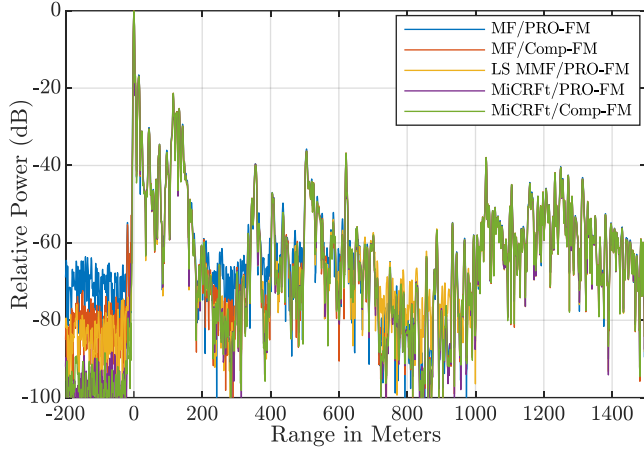


Fig. 10. Zero-Doppler slice of open-air measurements normalized relative to the direct path coupling between collocated transmit and receive antennas

Following standard Doppler processing, which includes simple projection-based clutter cancellation (since the platform is stationary), Figs. 11-15 and Table VI depict the range-Doppler response for each of the filter/waveform pairs. The range interval between roughly 1000 to 1300 meters includes multiple moving cars and trucks traversing the intersection. A useful metric in this case is the integrated range sidelobe modulation (IRSM), which is simply an average of the residual power over a range-Doppler region where RSM is prevalent.

Starting with the PRO-FM matched filter result in Fig. 11, what becomes immediately evident is the significant RSM that smears across Doppler out to about 700 meters. This RSM is a residual response from the direct path leakage that, though cancelled along with stationary clutter, still persists due to the nonstationarity of changing range sidelobes that remain visible given sufficient dynamic range. The IRSM in this region, excluding the clutter notch, is found to be -93.3 dBm. We shall use this value as the baseline to compare performance improvement for other filter/waveform pairs.

The use of Comp-FM waveforms and matched filtering in Fig. 12 reveals a noticeable reduction in overall RSM, enough so that the particular Doppler-smear RSM that is directly related to the range peaks at 0 and ~ 120 meters in Fig. 10 are now visible as horizontal streaks. The IRSM measured for this case (again excluding the clutter notch) is -102.8 dBm, a 9.5-dB reduction relative to the MF / PRO-FM case above. Further, the RSM-induced speckle in the vicinity of the traffic intersection in Fig. 11 is now significantly reduced as well.

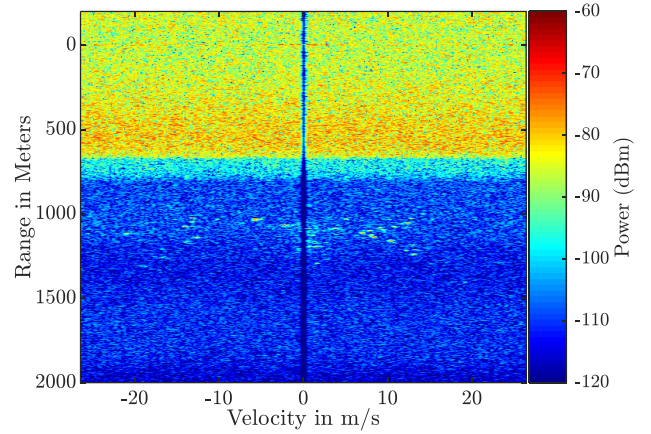


Fig. 11. Range-Doppler response for 1000 unique PRO-FM waveforms after pre-summing by 4, using matched filtering

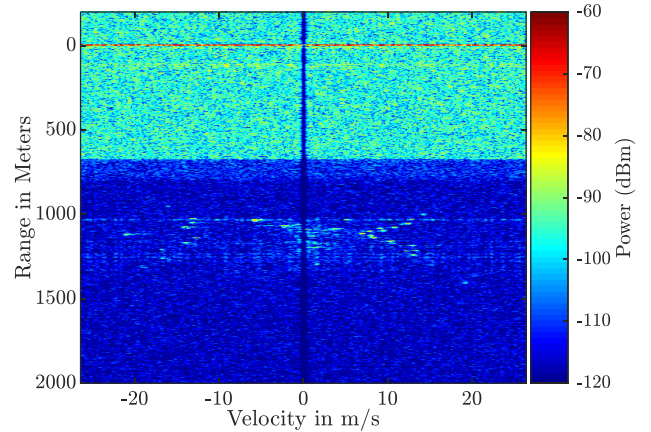


Fig. 12. Range-Doppler response for 250 unique Comp-FM subsets of $Z = 4$ waveforms, using matched filtering

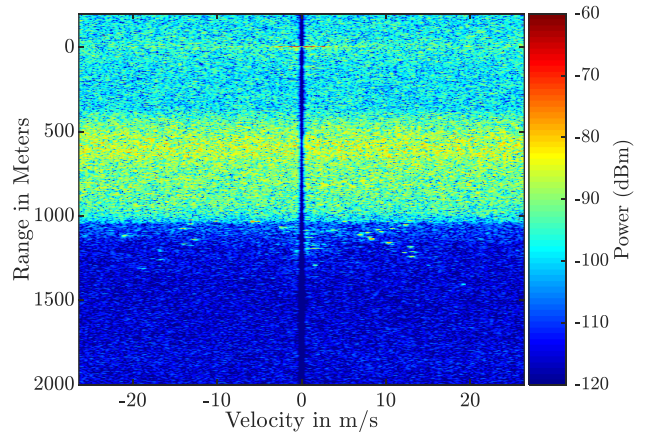


Fig. 13. Range-Doppler response for 1000 unique PRO-FM waveforms after pre-summing by 4, using individual MMFs via (34)

The individual MMF result in Fig. 13 likewise provides some reduction in RSM, though the impacted region is now greater due to the factor of $\kappa = 2$ extension in filter length, such that part of the intersection is now obscured. Moreover, the raised sidelobe region for the MMF corresponding to ± 4 μ s in Fig. 8 is readily apparent here in the vicinity of 600 meters in range, though the horizontal streaks noted in Fig. 12 are no longer visible. The IRSM in this case is -102.4 dBm, almost identical to the MF / Comp-FM case. That said,

the obscuration of the region of interest makes this approach qualitatively poorer.

Figures 14 and 15 illustrate the MiCRFt responses for PRO-FM and Comp-FM, respectively. Here we see that the RSM is almost completely removed, with the latter found to be marginally better by virtue of slightly more suppression of the residual direct path horizontal streaking effect noted above. In terms of IRSM these cases both achieve -119.5 dBm (a 26.2-dB improvement over the MF / PRO-FM baseline). The likely reason for these values being precisely the same is that the RSM has effectively been suppressed to the noise floor, thus precluding the further distinction observed in loopback in Table V.

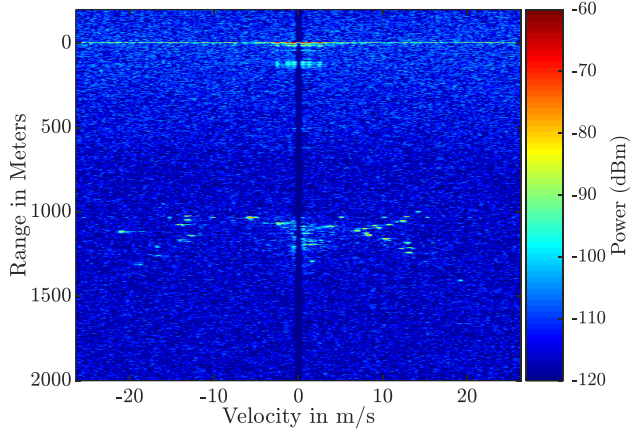


Fig. 14. Range-Doppler response for 1000 unique PRO-FM waveforms, using MiCRFt via (34) with $Q=4$

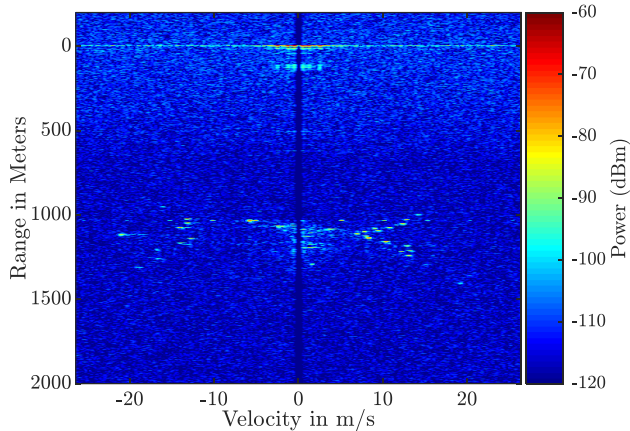


Fig. 15. Range-Doppler response for 250 unique Comp-FM subsets of $Z = 4$ waveforms, using MiCRFt via (34) with $Q=4$

Table VI. Integrated RSM comparison for Figs. 11-15

Filter / Waveform	Range-Doppler Integrated RSM	Improvement
MF / PRO-FM	-93.3 dBm	--
MF / Comp-FM	-102.8 dBm	9.5 dB
LS-MMF / PRO-FM	-102.4 dBm	9.1 dB
MiCRFT / PRO-FM	-119.5 dBm	26.2 dB
MiCRFT / Comp-FM	-119.5 dBm	26.2 dB

Figs. 16-20 present close-up versions of Figs. 11-15 that highlight the region of the traffic intersection. As noted above, the MF / PRO-FM case (Fig. 16) has some speckle that is induced by RSM, which is subsequently suppressed in the MF / Comp-FM case (Fig. 17), though a small degree of

Doppler smearing is observed near 1030 meters that is believed to be from a ventilation fan on a building within the field of view (per Google Earth).

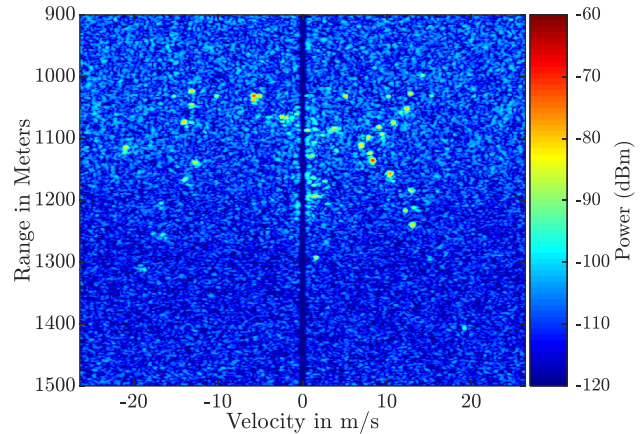


Fig. 16. Range-Doppler response for 1000 unique PRO-FM waveforms after pre-summing by 4, using matched filtering (intersection close-up)

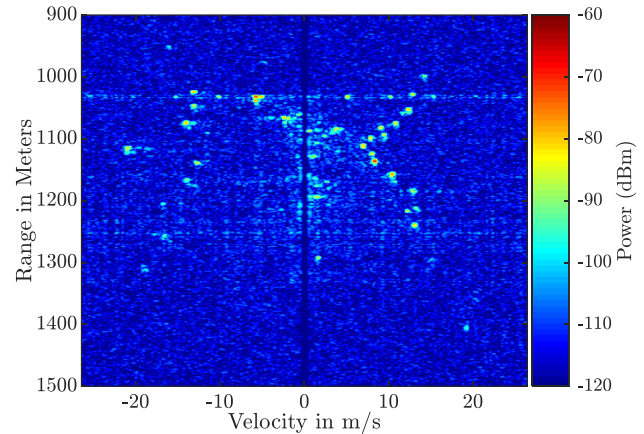


Fig. 17. Range-Doppler response for 250 unique Comp-FM subsets of $Z = 4$ waveforms, using matched filtering (intersection close-up)

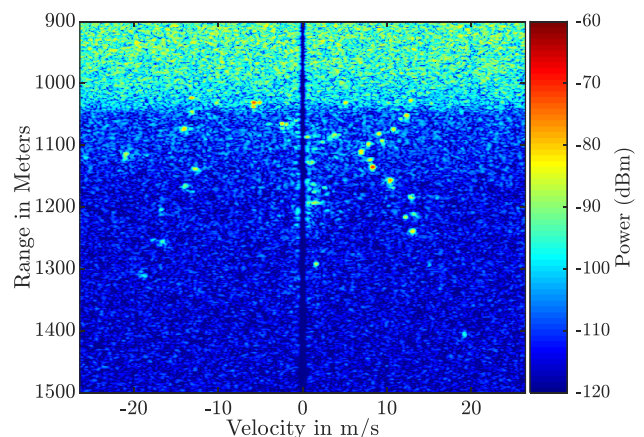


Fig. 18. Range-Doppler response for 1000 unique PRO-FM waveforms after pre-summing by 4, using individual MMFs via (34) (intersection close-up)

In Fig. 18 we see how the extended MMFs encroach upon the intersection, thus reducing sensitivity in this region. In contrast, in Figs. 19 and 20 the MiCRFt filters, which have the same extent as the individual MMFs, have basically

removed all trace of RSM from the intersection for both PRO-FM and Comp-FM waveforms.

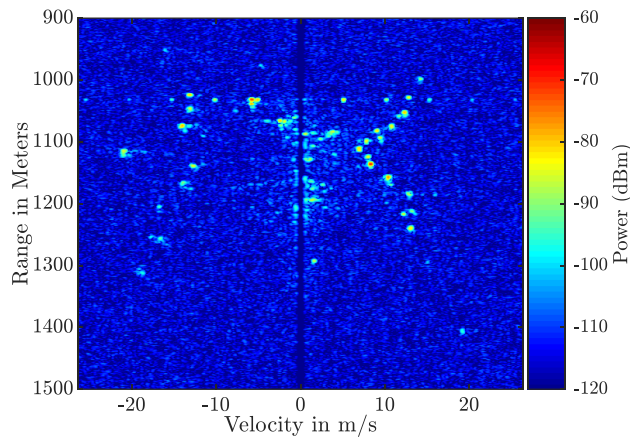


Fig. 19. Range-Doppler response for 1000 unique PRO-FM waveforms, using MiCRFt via (34) with $Q=4$ (intersection close-up)

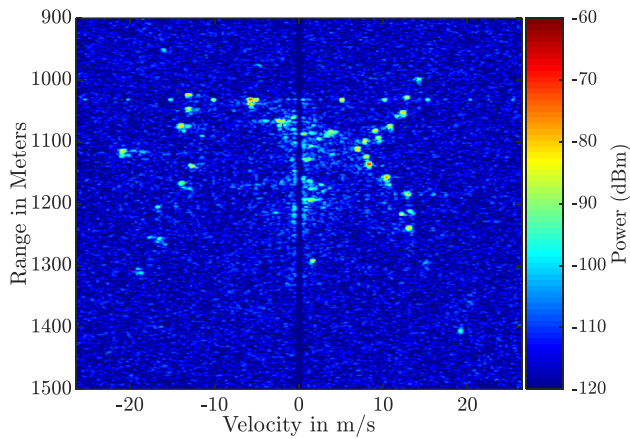


Fig. 20. Range-Doppler response for 250 unique Comp-FM subsets of $Z = 4$ waveforms, using MiCRFt via (34) with $Q=4$ (intersection close-up)

Finally, because random FM waveforms do provide an incoherent sidelobe averaging effect, it is also worth considering a smaller CPI within this complementary cancellation context. For the same measured data above, we now only use the first 100 pulses of each 1000-pulse CPI, resulting in 10 dB lower receive SNR and 10 dB less sidelobe reduction from averaging. Figs. 21-24 show the same close-up view of the traffic intersection, where significant RSM is visible in the PRO-FM scenarios when using MFs (Fig. 21) and the individual MMFs (Fig. 23). The Comp-FM (Fig. 22) and MiCRFt (Fig. 24) results once again show that RSM has been suppressed below the noise floor through the use of complementary waveforms or processing, respectively.

The result obtained by combining Comp-FM and MiCRFt (like Fig. 20) has been omitted because it appears identical to Figs. 22 and 24 due to the peak-power limit of our test setup. However, for a high-power radar operating requiring high dynamic range, the loopback results in Fig. 8 do suggest that this combination could prove useful. In short, this experimental demonstration of the capabilities enabled by Comp-FM waveforms and MiCRFt receive processing suggest that complementary operation may finally be within the realm of the feasible for some sensing applications.

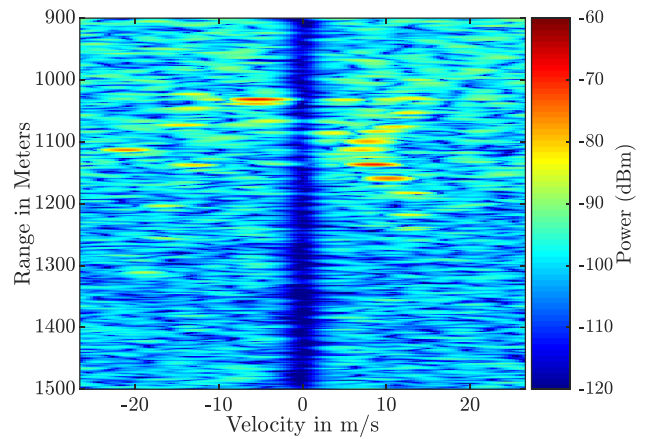


Fig. 21. Range-Doppler response for 100 unique PRO-FM waveforms after pre-summing by 4, using matched filtering (intersection close-up)

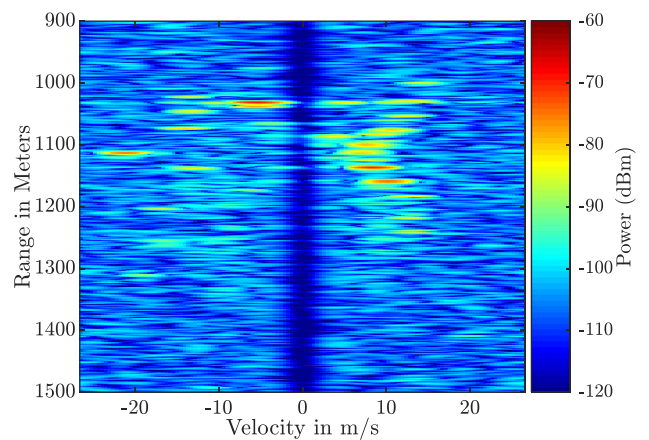


Fig. 22. Range-Doppler response for 25 unique Comp-FM subsets of $Z = 4$ waveforms, using matched filtering (intersection close-up)

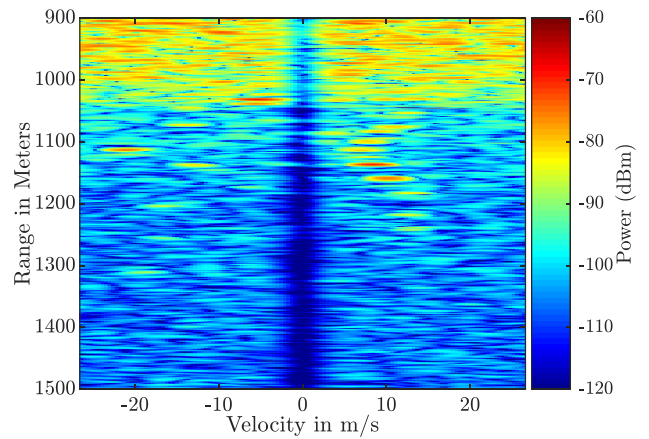


Fig. 23. Range-Doppler response for 100 unique PRO-FM waveforms after pre-summing by 4, using individual MMFs via (34) (intersection close-up)

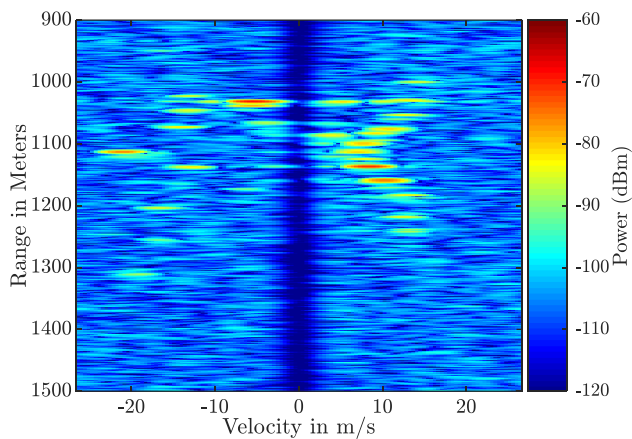


Fig. 24. Range-Doppler response for 100 unique PRO-FM waveforms, using MiCRFt via (34) with $Q=4$ (intersection close-up)

7. Conclusions

The notion of complementary coding has been around for several decades, though its practical application has been limited by Doppler degradation and transmitter effects. Here two new contributions to this field have been made that bridge the gap between the theoretical and the practical. Complementary FM (Comp-FM) waveform subsets are a sub-class of random FM that are amenable to the rigors of a radar transmitter, provide good complementary sidelobe cancellation, possess some robustness to Doppler effects, and degrade gracefully due to non-repetition of the subsets. Mismatched complementary-on-receive filtering (MiCRFt) provides a similar sidelobe cancellation capability when used in the context of nonrepeating waveforms. These approaches can likewise be combined for even further sidelobe suppression with almost negligible mismatch loss. Experimental loopback and open-air measurements have demonstrated the practical efficacy of these methods.

Finally, while outside the scope of consideration for this paper, the impact of multiple-time-around (MTA) echoes from the second (or further) range ambiguities is an interesting problem in the context of nonrepeating waveforms. While their high dimensionality may permit the separability required to reveal these more distant range intervals, the cancellation of MTA clutter introduces additional complexity (see [54]). Consequently, this research topic bears further investigation.

8. Acknowledgments

This work was supported by the Office of Naval Research under Contract #N00014-16-C-2029 and by a subcontract with Matrix Research, Inc. for the Air Force Research Laboratory under Prime Contract #FA8650-14-D-1722. DISTRIBUTION STATEMENT A. Approved for Public Release.

9. References

[1] Golay, M.J.E., "Complementary series," IRE Trans. Information Theory, vol. IT-7, no. 2, pp. 82-87, Apr. 1961.
 [2] Tseng, C.C., Liu, C.L., "Complementary sets of sequences," IEEE Trans. Information Theory, vol. IT-18, no. 5, pp. 644-652, Sept. 1972.

[3] Sivaswamy, R., "Digital and analog sub-complementary sequences for pulse compression," IEEE Trans. Aerospace & Electronic Systems, vol. AES-14, no. 2, pp. 343-350, Mar. 1978.
 [4] Sivaswamy, R., "Multiphase complementary codes," IEEE Trans. Information Theory, vol. IT-24, no. 5, pp. 546-552, Sept. 1978.
 [5] Frank, R.L., "Polyphase complementary codes," IEEE Trans. Information Theory, vol. IT-26, no. 6, pp. 641-647, Oct. 1980.
 [6] Luke, H.D., "Sets of one and higher dimensional Welchi codes and complementary codes," IEEE Trans. Aerospace & Electronic Systems, vol. AES-21, no. 2, pp. 170-179, Mar. 1985.
 [7] Budisin, S.Z., "New complementary pairs of sequences," IET Electronics Letters, vol. 26, no. 13, pp. 881-883, June 1990.
 [8] Bomer, L., Antweiler, M., "Periodic complementary binary sequences," IEEE Trans. Information Theory, vol. 36, no. 6, pp. 1487-1494, Nov. 1990.
 [9] Kretschmer, F.F., Gerlach, K., "Low sidelobe radar waveforms derived from orthogonal matrices," IEEE Trans. Aerospace & Electronic Systems, vol. 27, no. 1, pp. 92-102, Jan. 1991.
 [10] Mozeson, E., Levanon, N., "Removing autocorrelation sidelobes by overlaying orthogonal coding on any train of identical pulses," IEEE Trans. Aerospace & Electronic Systems, vol. 39, no. 2, pp. 583-603, Apr. 2003.
 [11] Fan, P., Yuan, W., Tu, Y., "Z-complementary binary sequences," IEEE Signal Processing Letters, vol. 14, no. 8, pp. 509-512, Aug. 2007.
 [12] Pezeshki, A., Calderbank, A.R., Moran, W., Howard, S.D., "Doppler resilient Golay complementary waveforms," IEEE Trans. Information Theory, vol. 54, no. 9, pp. 4254-4266, Sept. 2008.
 [13] Bi, J., Rohling, H., "Complementary binary code design based on mismatched filter," IEEE Trans. Aerospace & Electronic Systems, vol. 48, no. 2, pp. 1793-1797, Apr. 2012.
 [14] Song, J., Babu, P., Palomar, D.P., "Sequence set design with good correlation properties via majorization-minimization," IEEE Trans. Signal Processing, vol. 64, no. 11, pp. 2866-2879, June 2016.
 [15] Nguyen, H.D., Coxson, G.E., "Doppler tolerance, complementary code sets, and generalised Thue-Morse sequences," IET Radar, Sonar & Navigation, vol. 10, no. 9, pp. 1603-1610, Dec. 2016.
 [16] Levanon, N., Cohen, I., Itkin, P., "Complementary pair radar waveforms – evaluating and mitigating some drawbacks," IEEE Aerospace & Electronic Systems Mag., vol. 32, no. 3, pp. 40-50, Mar. 2017.
 [17] Levanon, N., Mozeson, E., Radar Signals, Wiley – IEEE Press, 2004.

- [18] Blunt, S.D., Mokole, E.L., "An overview of radar waveform diversity," *IEEE Aerospace & Electronic Systems Mag.*, vol. 31, no. 11, pp. 2-42, Nov. 2016.
- [19] Griffiths, H., Cohen, L., Watts, S., Mokole, E., Baker, C., Wicks, M., Blunt, S., "Radar spectrum engineering and management: technical and regulatory issues," *Proc. IEEE*, vol. 103, no. 1, pp. 85-102, Jan. 2015.
- [20] Chen, R., Cantrell, B., "Highly bandlimited radar signals," *IEEE Radar Conf.*, Pasadena, CA, May 2002.
- [21] Faust, H., Connolly, B., Firestone, T.M., Chen, R.C., Cantrell, B.H., Mokole, E.L., "A spectrally clean transmitting system for solid state phased-array radars," *IEEE Radar Conf.*, Philadelphia, PA, Apr. 2004.
- [22] Taylor, J.W., Blinchikoff, H.J., "Quadruphase code – a radar pulse compression signal with unique characteristics," *IEEE Trans. Aerospace & Electronic Systems*, vol. 24, no. 2, pp. 156-170, Mar. 1988.
- [23] Blunt, S.D., Cook, M., Jakabosky, J., Graaf, J.D., Perrins, E., "Polyphase-coded FM (PCFM) radar waveforms, part I: implementation," *IEEE Trans. Aerospace & Electronic Systems*, vol. 50, no. 3, pp. 2218-2229, July 2014.
- [24] Blunt, S.D., Jakabosky, J., Cook, M., Stiles, J., Sequin, S., Mokole, E.L., "Polyphase-coded FM (PCFM) radar waveforms, part II: optimization," *IEEE Trans. Aerospace & Electronic Systems*, vol. 50, no. 3, pp. 2230-2241, July 2014.
- [25] Anderson, J.B., Aulin, T., Sundberg, C.-E., *Digital Phase Modulation*, Plenum Press, New York, NY, 1986.
- [26] Blunt, S.D., Cook, M., Perrins, E., de Graaf, J., "CPM-based radar waveforms for efficiently bandlimiting a transmitted spectrum," *IEEE Radar Conf.*, Pasadena, CA, USA, May 2009.
- [27] Mohr, C.A., McCormick, P.M., Blunt, S.D., "Optimized complementary waveform subsets within an FM noise radar CPI," *IEEE Radar Conf.*, Oklahoma City, OK, USA, Apr. 2018.
- [28] Blunt, S.D., Jakabosky, J.K., Mohr, C.A., McCormick, P.M., Owen, J.W., Ravenscroft, B., Sahin, C., Zook, G.D., Jones, C.C., Metcalf, J.G., Higgins, T., "Principles & applications of random FM radar waveform design," to appear in *IEEE Aerospace & Electronic Systems Mag.*
- [29] Blunt, S.D., Cook, M.R., Stiles, J., "Embedding information into radar emissions via waveform implementation," *Intl. Waveform Diversity & Design Conf.*, Niagara Falls, Canada, Aug. 2010.
- [30] Sahin, C., Metcalf, J., Blunt, S., "Characterization of range sidelobe modulation arising from radar-embedded communications," *IET Intl. Conf. Radar Systems*, Belfast, UK, Oct. 2017.
- [31] Ackroyd, M.H., Ghani, F., "Optimum mismatched filters for sidelobe suppression," *IEEE Trans. Aerospace & Electronic Systems*, vol. AES-9, no. 2, pp. 214-218, Mar. 1973.
- [32] Henke, D., McCormick, P., Blunt, S.D., Higgins, T., "Practical aspects of optimal mismatch filtering and adaptive pulse compression," *IEEE Intl. Radar Conf.*, Arlington, VA, USA, May 2015.
- [33] Jakabosky, J., Blunt, S.D., Hamed, B., "Spectral-shape optimized FM noise radar for pulse agility," *IEEE Radar Conf.*, Philadelphia, PA, USA, May 2016.
- [34] Sahin, C., Metcalf, J., Blunt, S., "Filter design to address range sidelobe modulation in transmit-encoded radar-embedded communications," *IEEE Radar Conf.*, Seattle, WA, USA, May 2017.
- [35] Ravenscroft, B., McCormick, P.M., Blunt, S.D., Perrins, E., Metcalf, J.G., "A power-efficient formulation of tandem-hopped radar & communications," *IEEE Radar Conf.*, Oklahoma City, OK, USA, Apr. 2018.
- [36] Mohr, C.A., McCormick, P.M., Blunt, S.D., Mott, C., "Spectrally efficient FM noise radar waveforms optimized in the logarithmic domain," *IEEE Radar Conf.*, Oklahoma City, OK, USA, Apr. 2018.
- [37] Mohr, C.A., Blunt, S.D., "FM noise waveforms optimized according to a temporal template error (TTE) metric," *IEEE Radar Conf.*, Boston, MA, USA, Apr. 2019.
- [38] Mohr, C.A., Blunt, S.D., "Design and generation of stochastically defined, pulsed FM noise waveforms," *Intl. Radar Conf.*, Toulon, France, Sept. 2019.
- [39] Jones, C.C., Blunt, S.D., "Mismatched complementary-on-receive filtering of diverse FM waveform subsets," *Intl. Radar Conf.*, Toulon, France, 23-27 Sept. 2019.
- [40] Tan, P.S., Jakabosky, J., Stiles, J.M., Blunt, S.D., "Higher-order implementations of polyphase-coded FM radar waveforms," *IEEE Trans. Aerospace & Electronic Systems*, vol. 55, no. 6, pp. 2850-2870, Dec. 2019.
- [41] Klein, A.M., Fujita, M.T., "Detection performance of hard-limited phase-coded signals," *IEEE Trans. Aerospace & Electronic Systems*, vol. AES-15, no. 6, pp. 795-802, Nov. 1979.
- [42] Richards, M.A., Scheer, J.A., Holm, W.A., *Principles of Modern Radar: Basic Principles*, SciTech Publishing, pp. 786-787, 2010.
- [43] McCormick, P.M., Blunt, S.D., "Nonlinear conjugate gradient optimization of polyphase-coded FM radar waveforms," *IEEE Radar Conf.*, Seattle, WA, May 2017.
- [44] Mohr, C.A., McCormick, P.M., Topliff, C.A., Blunt, S.D., Baden, J.M., "Gradient-based optimization of PCFM radar waveforms," to appear in *IEEE Trans. Aerospace & Electronic Systems*.
- [45] McCormick, P.M., Blunt, S.D., "Gradient-based coded-FM waveform design using Legendre polynomials," *IET Intl. Conf. Radar Systems*, Belfast, UK, Oct. 2017.
- [46] Mohr, C.A., Blunt, S.D., "Analytical spectrum representation for physical waveform optimization requiring extreme fidelity," *IEEE Radar Conf.*, Boston, MA, Apr. 2019.
- [47] Owen, J., Mohr, C., Blunt, S.D., Gallagher, K., "Nonlinear radar via intermodulation of jointly optimized FM noise waveform pairs," *IEEE Radar Conf.*, Boston, MA, Apr. 2019.

- [48] Baden, J.M., O'Donnell B., Schmieder, L., "Multiobjective sequence design via gradient descent methods," IEEE Trans. Aerospace & Electronic Systems, vol. 54, no. 3, pp. 1237-1252, June 2018.
- [49] Ghadimi, E., Feyzmahdavian, R., Johansson, M., "Global convergence of the heavy-ball method for convex optimization," European Control Conf., Linz, Austria, July 2015.
- [50] Nocedal, J., Wright, S., Numerical Optimization. Springer Science & Business Media, 2006.
- [51] Jakabosky, J., Blunt, S.D., Himed, B., "optimization of "over-coded" radar waveforms," IEEE Radar Conf., Cincinnati, OH, USA, May 2014.
- [52] Sahin, C., Jakabosky, J., McCormick, P., Metcalf, J., Blunt, S., "A novel approach for embedding communication symbols into physical radar waveforms," IEEE Radar Conf., Seattle, WA, May 2017.
- [53] Raab, F.H., Asbeck, P., Cripps, S., Kenington, P.B., Popovic, Z.B., Potheary, N., Sevic, J.F., Sokal, N.O., "Power amplifiers and transmitters for RF and microwave," IEEE Trans. Microwave Theory & Techniques, vol. 50, no. 3, pp. 814-826, Mar. 2002.
- [54] Higgins, T., Gerlach, A.K., Shackelford, A.K., Blunt, S.D., "Aspects of non-identical multiple pulse compression," IEEE Radar Conf., Kansas City, MO, May 2011.